Nano Research 2018, 11(6): 3362–3370
https://doi.org/10.1007/s12274-017-1933-4
Research Article
ISSN 1998-0124
CN 11-5974/O4

Surface-adsorbed ions on TiO_2 nanosheets for selective photocatalytic CO_2 reduction

Xiaogang Li[1,§], Wentuan Bi[1,§], Zhe Wang[2,§], Wenguang Zhu[2], Wangsheng Chu[3] (✉), Changzheng Wu[1] (✉), and Yi Xie[1]

[1] *Hefei National Laboratory for Physical Sciences at the Microscale, iChEM (Collaborative Innovation Center of Chemistry for Energy Materials), and CAS Key Laboratory of Mechanical Behavior and Design of Materials, University of Science and Technology of China, Hefei 230026, China*

[2] *International Center for Quantum Design of Functional Materials (ICQD), Hefei National Laboratory for Physical Sciences at the Microscale (HFNL), Synergetic Innovation Center of Quantum Information and Quantum Physics, Department of Physics, and Key Laboratory of Strongly-Coupled Quantum Matter Physics, Chinese Academy of Sciences, School of Physical Sciences, University of Science and Technology of China, Hefei 230026, China*

[3] *National Synchrotron Radiation Laboratory, University of Science and Technology of China, Hefei 230026, China*

[§] *Xiaogang Li, Wentuan Bi and Zhe Wang contributed equally to this work.*

Received: 14 September 2017
Revised: 20 November 2017
Accepted: 22 November 2017

KEYWORDS
two-dimensional nanomaterials,
surface modification,
ion adsorption,
photocatalysis,
TiO_2 nanosheets

ABSTRACT

A method based on the adsorption of ions on the surface of two-dimensional (2D) nanosheets has been developed for photocatalytic CO_2 reduction. Isolated Bi ions, confined on the surface of TiO_2 nanosheets using a simple ionic adsorption method facilitate the formation of a built-in electric field that effectively promotes charge carrier separation. This leads to an improved performance of the photocatalytic CO_2 reduction process with the preferred conversion to CH_4. The proposed surface ion-adsorption method is expected to provide an effective approach for the design of highly efficient photocatalytic systems. These findings could be very valuable in photocatalytic CO_2 reduction applications.

1 Introduction

The excessive depletion of fossil fuels has led to a global energy crisis and environmental challenges; the atmospheric accumulation of CO_2 (a greenhouse gas) has triggered increasing concerns [1–3]. The

Address correspondence to Changzheng Wu, czwu@ustc.edu.cn; Wangsheng Chu, chuws@ustc.edu.cn

photocatalytic conversion of CO_2 into energy-rich chemicals is considered a promising approach to replace fossil fuels and reduce the emission of CO_2 [4–6]. Despite recent progress, the photoconversion of CO_2 still suffers from a low efficiency due to the significant recombination of charge carriers of the photocatalysts [7, 8]. In addition, the selectivity required for carbonaceous products poses challenges in the design of the photocatalysts for product separation [9]. Therefore, the development of highly efficient and selective photocatalysts for CO_2 reduction is of a key importance.

The introduction of heterogeneous ions to catalysts is an effective strategy to tune the CO_2 reduction activity by virtue of their improved light harvesting and modulated charge transfer characteristics [10–12]. However, the doping ions in the bulk can act as recombination centers and hinder carrier migration, which is detrimental in the design of highly efficient photocatalytic systems [13]. Recently, two-dimensional (2D) nanosheets have been considered promising for photocatalysis owing to their rich active sites and shortened carrier transfer distances [14–18]. In addition, for 2D nanomaterials having atomic-scale thicknesses, the surface phases are as important as those in the bulk; this provides an alternative approach to engineer their intrinsic physicochemical properties by simply modifying the surface [19–24]. Therefore, the surface modification of 2D nanomaterials by the introduction of heterogeneous ions may provide a reliable model system for the design of photocatalysts for CO_2 reduction [25–27].

In this study, we demonstrated a surface ion adsorption method by confining isolated Bi ions on the surface of 2D TiO_2 for photocatalytic CO_2 reduction. The whole synthetic process is remarkably simple, convenient, and can be easily scaled up. The Bi ions which are adsorbed on the surface could induce a built-in electric field. This effectively facilitates charge carrier transfer and improves photocatalytic CO_2 reduction performance. The Bi ions on the TiO_2 nanosheets permit the preferred conversion of CO_2 to CH_4 through a cascade catalysis. We anticipate that the proposed surface ion adsorption method of adsorbing ions on the surface of catalysts will provide a novel approach for the design of highly efficient photocatalytic systems for CO_2 reduction.

2 Results and discussion

The synthetic process of TiO_2 nanosheets with Bi ions adsorbed on the surface (TiO_2-Bi) is illustrated in Fig. 1(a). The morphology of TiO_2 and TiO_2-Bi was revealed using transmission electron microscopy (TEM). Figures S1(a) and S1(b) in the Electronic Supplementary Material (ESM) show that both TiO_2 and TiO_2-Bi exhibit rectangular sheet structures with similar size and thickness. It is worth noting that no particles were observed on the surface of the TiO_2-Bi. The X-ray diffraction (XRD) patterns in Fig. S2 in the ESM show that TiO_2 and TiO_2-Bi have the same crystal structure which corresponds to that of anatase TiO_2 (JCPDS No. 21-1272). The TEM and XRD characterizations indicated that the introduction of Bi ions has almost no effects on the morphology and crystal structure of TiO_2.

As a powerful tool for discerning individual heavy atoms [28], high-angle annular dark-field scanning transmission electron microscopy (HAADF-STEM) was employed to reveal the presence and configuration of the Bi ions on the TiO_2 structure. The HAADF-STEM image in Fig. 1(b) shows isolated bright spots that correspond to the Bi ions dispersed on TiO_2. This confirms the existence of isolated Bi atoms on the TiO_2 nanosheets. In order to reveal the local chemical environment around a Bi atom, extended X-ray absorption fine structure (EXAFS) spectrometry was performed at the Ti K-edge and Bi L_3-edge. The TiO_2-Bi shows identical Fourier transform (FT)-EXAFS curves with those of the supported TiO_2 at the Ti K-edge, as shown in Figs. S3(a) and S3(b) in the ESM. This indicates that the local geometrical structure of the TiO_2 support has not considerably changed with the introduction of Bi. In contrast, the Bi L_3-edge EXAFS spectra of the TiO_2-Bi sample exhibit completely different oscillations compared with those of the Bi_2O_3 reference sample. Figure S4 in the ESM shows that the EXAFS oscillations of the TiO_2-Bi behave almost as a single sine wave, while the EXAFS curves of the Bi_2O_3 sample exhibit finer oscillations, as outlined by the arrows in the figure. The k^2-weighted Fourier transform shown in Fig. 1(c) additionally demonstrates

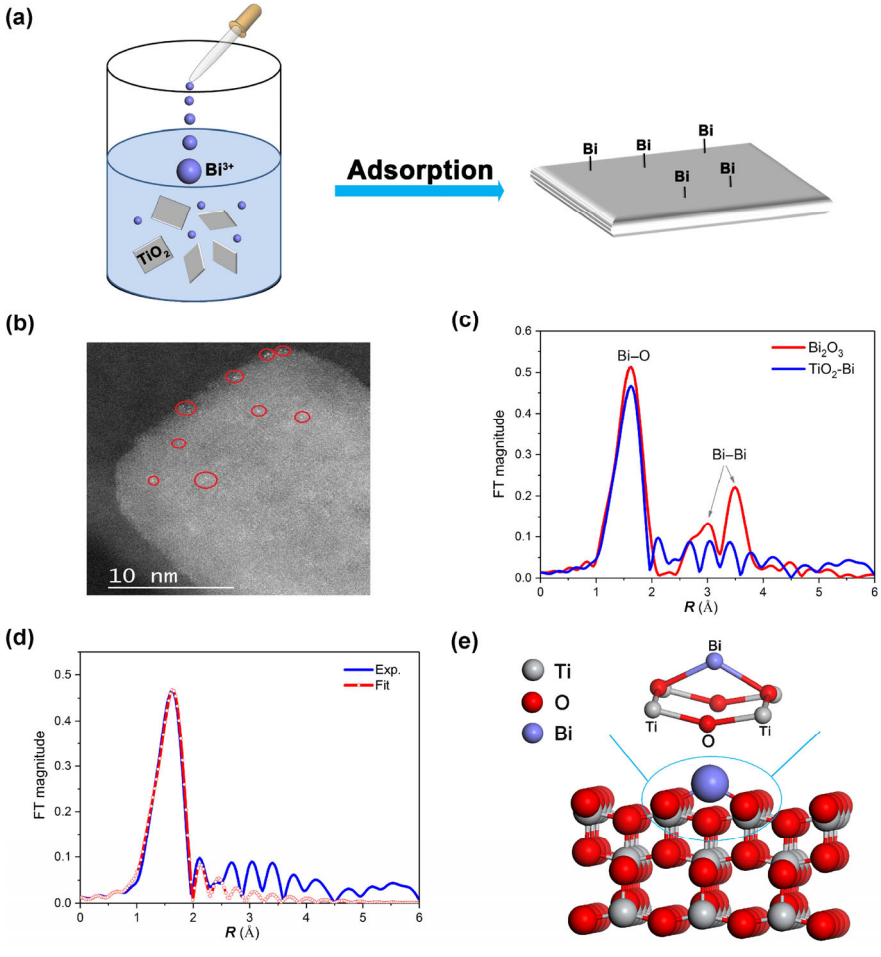

Figure 1 (a) Illustration of the TiO_2-Bi synthetic process. (b) HAADF-STEM image of TiO_2-Bi. (c) Fourier transforms of the Bi L_3-edge EXAFS oscillations of TiO_2-Bi and Bi_2O_3. (d) Comparison of the FT-EXAFS curves between the experimental data and fitting results of the TiO_2-Bi. (e) Model of the TiO_2-Bi structure.

the above behavior. For the TiO_2-Bi sample, only one significant peak was detected at a distance of 1.62 Å (no phase corrections), which emerges from the interactions with the first nearest oxygen atoms (Bi–O). It can be noticed that for distances larger than 2.0 Å, no considerable peaks can be distinguished from the background noise. This suggests that the isolated Bi ions were confined to the surface of TiO_2. The figure shows almost equal distances of the Bi–O peaks of TiO_2-Bi and Bi_2O_3 in the FT curves. This indicates that the Bi–O bond length in TiO_2-Bi is equal to that in Bi_2O_3. The slight decrease of the Bi–O peak intensity of the TiO_2-Bi sample suggests that the coordination number of oxygen is decreased or that the disorder of the oxygen shell is larger. In order to quantitatively obtain the local atomic arrangement of Bi on the TiO_2 surface, EXAFS data were fitted in the *R*-space (Fig. 1(d)). The obtained structural parameters are listed in Table S1 in the ESM. The fitting results show that the coordination number of the oxygen atoms in the Bi-TiO_2 sample is slightly smaller, while the average distance to the oxygen atoms around Bi is slightly larger, compared with those in the Bi_2O_3 reference sample. Using the EXAFS results, we propose a structural model of the TiO_2-Bi structure, where an isolated Bi bonds with two O atoms on the surface of TiO_2, as shown in Fig. 1(e).

The influence of Bi ions on the photocatalytic CO_2 reduction activity of TiO_2 is presented in Fig. 2. Figure 2(a) shows that the TiO_2-Bi exhibits an enhanced CO_2 reduction activity, compared with blank TiO_2. During the 14 h-test, the TiO_2-Bi provides stable evolutions of CH_4 and CO, which indicates the stability of the TiO_2-Bi. The TEM image and XRD

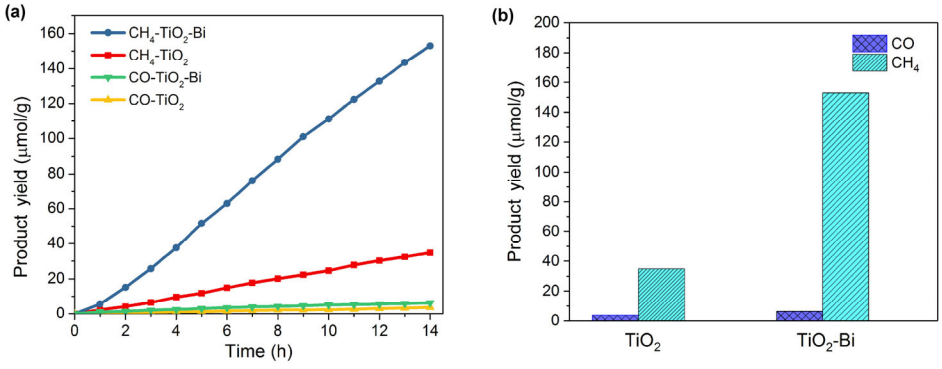

Figure 2 (a) Comparison between the photocatalytic CO_2 reduction performances of TiO_2 and TiO_2-Bi. (b) Variation in the amount of CO and CH_4 during the 14 h-long test process.

pattern shown in Fig. S5 in the ESM indicate that TiO_2-Bi after the photocatalytic reaction preserves the initial morphology and crystal structure, which additionally demonstrates its stability. The amount of CH_4 and CO during the 14-h-long test process is illustrated in Fig. 2(b). The TiO_2-Bi provides 6.38 μmol/g CO and 153.08 μmol/g CH_4, while the blank TiO_2 provides 3.74 μmol/g CO and 34.86 μmol/g CH_4 in 14 h. It is worth noting that compared with the 1.7 times improved conversion performance for CO, TiO_2-Bi exhibits preferred conversion for CH_4, as it is improved 4.4 times, compared to the blank TiO_2.

To gain further insights into the improved activity of TiO_2-Bi, we performed ultraviolet–visible (UV–vis) absorption spectroscopy to evaluate the optical properties of the samples. As shown in Fig. S6(a) in the ESM, the absorption edge of TiO_2 is observed at approximately 388 nm, which corresponds to a band gap of 3.19 eV. TiO_2-Bi shows an absorption edge at 390 nm, which corresponds to a band gap of 3.18 eV. It is clear that the absorption of light by TiO_2 exhibits no obvious change after the introduction of Bi ions on the surface. It could be expected that the low amount of Bi has little effect on the light absorption. Therefore, the enhanced photocatalytic performance of TiO_2-Bi is not solely attributed to the light absorption. Further, we performed photoluminescence (PL) spectroscopy to evaluate the efficiency of charge carrier separation. As shown in Fig. S6(b) in the ESM, the introduction of Bi ions on the surface causes a remarkable decrease of the PL intensity. This demonstrates that the isolated Bi ions suppress the recombination of charge carriers.

In order to further study the transfer process of charge carriers, we perform lock-in based surface photovoltage (SPV) measurements, which are very suitable for the analysis of photoinduced charge transfer in nanomaterials with high sensitivity [29, 30]. As shown in Fig. 3(a), for both TiO_2 and TiO_2-Bi, when the wavelength is smaller than 400 nm, a strong SPV response is observed, caused by the intrinsic band to band transitions, which depends on the band gap. TiO_2-Bi shows a higher SPV response than TiO_2, which demonstrates the more effective separation of the charge carriers [31, 32]. It is worth noting that both TiO_2 and TiO_2-Bi have a weak SPV response between 400–800 nm, which can be attributed to the surface states [33]. In order to reveal the charge carriers transfer process, which is correlated with the surface states, we performed SPV phase spectroscopy. As illustrated in Fig. 3(b), the phase values of TiO_2 and TiO_2-Bi are between 90° and 180° in the range of ~ 400–800 nm. This causes a negative value of cos(ϕ), which indicates the accumulation of a negative charge at the surface [34, 35]. Therefore, the SPV signal in the range of 400–800 nm emerges owing to the electron transfer to the surface. Figure 3(a) shows that TiO_2-Bi exhibits a higher SPV response than TiO_2 in the range of 400–800 nm. This demonstrates that the transfer of photogenerated electrons to the surface of TiO_2 is enhanced by the introduction of Bi atoms. The SPV characterization additionally confirms that the isolated Bi atoms, confined on the surface of TiO_2, could promote the transfer of photogenerated electrons to the surface with a high efficiency of separation of charge

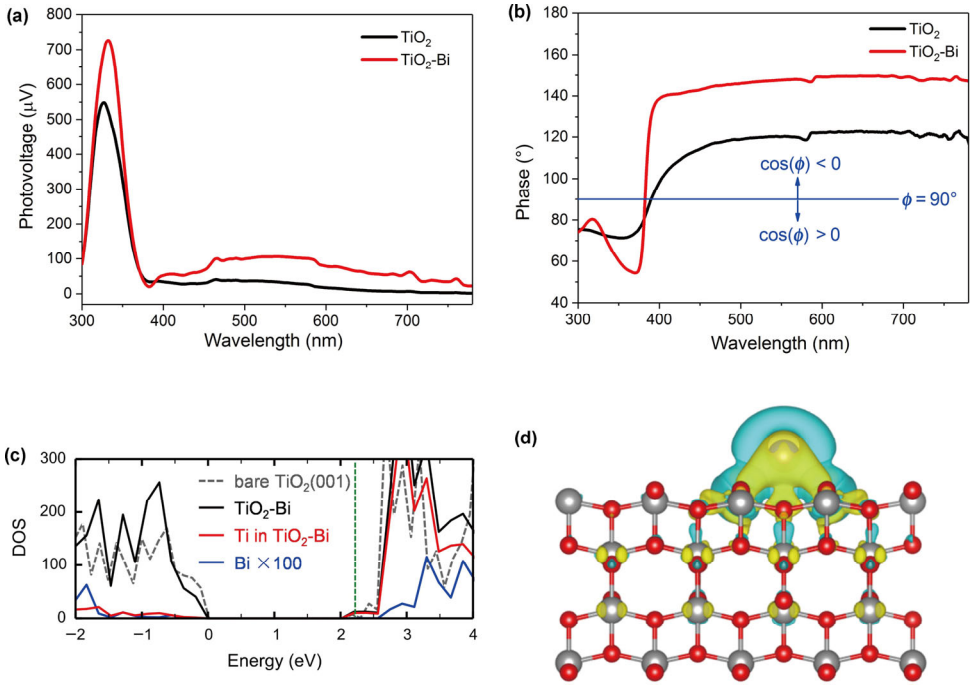

Figure 3 (a) SPV spectroscopy measurements of TiO_2 and TiO_2-Bi. (b) Corresponding SPV phase spectroscopy measurements of TiO_2 and TiO_2-Bi. (c) Total DOS of bare TiO_2 and TiO_2-Bi, and site-projected DOS on the Ti and Bi in TiO_2-Bi. The valence band maximum of bare TiO_2 is set to zero. The green dashed line indicates the Fermi-level of TiO_2-Bi. (d) The charge density difference in TiO_2-Bi. The regions of electron accumulation and depletion are outlined in yellow and blue, respectively.

carriers, thus facilitating the subsequent photocatalytic reaction.

In order to understand the mechanism of the observed accelerated charge transfer in TiO_2-Bi and reveal its electronic structure, we performed density functional theory (DFT) calculations. The adsorption structure of the Bi ions on the TiO_2 (001) surface is confirmed to be stable, as illustrated in Fig. 1(e). Figure 3(c) shows the density of states (DOS) of the TiO_2 (001) surfaces with and without the Bi surface adsorption. The energy of the valence band maximum of the blank TiO_2 substrate is set to zero. The energy bands of the two systems are aligned with respect to the core level of a Ti atom that is far away from the surface. Compared with the DOS of the blank TiO_2 substrate, the DOS of TiO_2-Bi does not show an obvious difference in the vicinity of the band gap region, whereas the Fermi-level of the TiO_2-Bi structure shifts into the conduction band. The site-projected DOS at the Ti and Bi reveal that the occupied states in the conduction band correspond to Ti, which indicates that electrons transfer from Bi to TiO_2 upon the Bi adsorption. This can be further confirmed by the charge density difference plot, as shown in Fig. 3(d), where the charge density difference is calculated by subtracting the total charge densities of an isolated Bi ion and blank TiO_2 substrate from that of the combined TiO_2-Bi. The electron transfer from the Bi ions to the TiO_2 substrate is expected to induce an electric field from the surface to the interior of the TiO_2 substrate, which could effectively promote a separation of the photon-generated charge carriers, as revealed by the above SPV and PL spectroscopy measurements.

As mentioned above, TiO_2-Bi exhibits a preferred conversion of CO_2 to CH_4. One well-accepted route for the formation of CH_4 is through the consecutive transfer of protons and electrons to CO, which is the intermediate product during the CO_2 reduction process [5, 36]. In other words, the preferred conversion to CH_4 of the TiO_2-Bi emerges from its improved activity in the CO reduction process. In order to confirm the above arguments, we performed a photocatalytic CO reduction test. As shown in Fig. 4(a), TiO_2-Bi provides a CH_4 evolution rate of 4.1 μmol/(g·h), 5.6 times larger than that for the blank TiO_2 which provides a CH_4 evolution rate of 0.78 μmol/(g·h).

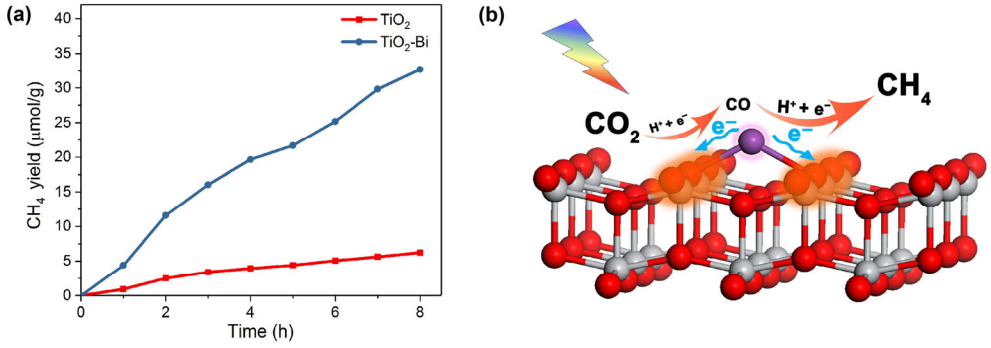

Figure 4 (a) Photocatalytic CO reduction activities of TiO_2 and TiO_2-Bi. (b) Schematic of the CO_2 reduction process.

Therefore, we could conclude that the accelerated charge transfer in TiO_2-Bi facilitates the CO reduction, which eventually leads to a preferred conversion of CH_4, as illustrated in Fig. 4(b).

3 Conclusions

We proposed a surface ion adsorption method that provides enhanced CO_2 reduction activities for 2D photocatalysts. The Bi ions adsorbed on the surface of TiO_2 nanosheets act as electron donors that induce charge redistribution on the surface of TiO_2. This is expected to generate a built-in electric field that contributes to the separation of charge carriers. The accelerated charge transfer facilitates the further reduction of CO, eventually leading to a preferred CO_2 reduction to CH_4. We believe that the surface ion adsorption method could provide an effective approach for the design of highly efficient photocatalytic systems that are of significance in CO_2 reduction applications.

4 Methods

4.1 Preparation of TiO_2 nanosheets

The TiO_2 nanosheets exposed (001) facets are prepared by employing a hydrothermal method, similar to that reported by Xie et al. [37]. First, 12.5 mL of $Ti(OC_4H_9)_4$ and 1.5 mL of a hydrofluoric acid solution (concentration ~ 40 wt.%) were mixed in a dried Teflon-lined autoclave that has a capacity of 50 mL, followed by a hydrothermal treatment of the mixture at 180 ℃ for 24 h. Then, the system was allowed to naturally cool down to room temperature. The final product was collected by centrifuging the mixture, washed several times with 0.1 M NaOH, distilled water, and ethanol, and then dried overnight in a vacuum at 60 ℃.

4.2 Preparation of TiO_2-Bi

First, 0.1 mmol $BiCl_3$ was dissolved into 0.5 M HCl solution, followed by addition of 50 mg as-synthesized TiO_2. The mixture was sonicated into a homogeneous solution. The solution was stirred at least 6 h and then kept standing overnight. Then, we poured the supernatant and transferred the bottom precipitate into an alumina boat with ethanol, followed by heating at 80 ℃ for 1 h in Ar atmosphere in order to dry the sample. Then, it was further heated at 200 ℃ for 1 h. The cooled sample was then washed with a diluted HCl solution to remove the extra $BiCl_3$, and further washed several times with distilled water and ethanol. Then, it was dried in a vacuum at 60 ℃ overnight for a further characterization.

4.3 Photocatalytic activity measurements

The photocatalytic CO_2 reduction performance was evaluated in a gas-closed circulation system equipped with a vacuum line. A 100 mg photocatalyst powder was put in a glass reactor filled with CO_2, followed by an injection of 2 mL H_2O and then illuminated using a 300 W Xe lamp (PLS-SXE300/300UV, Trusttech Co., Ltd.). The amounts of CO and CH_4 were determined by performing gas chromatography (Agilent 7890B). The measurement method for the photocatalytic CO reduction performance is the same as that for the CO_2 reduction.

4.4 Characterization

TEM images were acquired using an H-7650 (Hitachi, Japan) microscope operated at an acceleration voltage of 100 kV. The powder XRD was performed using a Philips X'Pert Pro Super diffractometer with a graphite monochromatized Cu-Kα radiation (λ = 1.54178 Å). The HAADF-STEM measurements were performed using a JEOL JEM-ARF200F TEM/STEM equipped with a spherical aberration corrector. Steady-state UV–Vis absorption spectra were recorded using a Perkin Elmer Lambda 950 spectrophotometer. PL emission spectra were obtained using a FLUOROLOG-3-TAU fluorescence spectrometer (Horiba) upon excitation at 300 nm. The SPV spectra measurements were performed using a lock-in amplifier. The measurement system consisted of a monochromatic light, lock-in amplifier (SR830–DSP) with a light chopper (SR540), photovoltaic cell, and computer. The monochromatic light was provided by passing the light from a 500 W xenon lamp (CHF-XM500, Trusttech Co., Ltd.) through a grating monochromator (Omni-3007, No. 16047, Zolix).

The Bi L_3-edge and Ti K-edge EXAFS data were collected at the beamline 1W1B of the Beijing Synchrotron Radiation Facility (BSRF, Beijing) and at the beamline 14W1 of the Shanghai Synchrotron Radiation Laboratory (SSRL, Shanghai) at room temperature. The typical energies of the storage ring were 2.5 GeV (BSRF) and 3.5 GeV (SSRF). A Ti foil was used to calibrate the Si (111) double crystal monochromator, and then it was used to collect EXAFS data for the reference spectrum. The Ti K-edge EXAFS data of TiO_2 and TiO_2-Bi and Bi L_3-edge EXAFS data of the Bi_2O_3 reference sample were measured in the transmission mode by mixing the sample with a graphite powder, which was then pressed into a disc that has a diameter of 10 mm. The Bi L_3-edge EXAFS data of TiO_2-Bi were collected in the fluorescence mode using a Lytle detector by pressing the sample into the disc that has a diameter of 10 mm.

4.5 Computational methods

First-principles calculations were performed using the Vienna *ab-initio* simulation package (VASP) [38], which is based on DFT and plane wave basis sets; the projector-augmented wave (PAW) method was employed [39, 40]. The employed exchange correlation functional was obtained using the Perdew–Burke–Ernzerhof (PBE) [41] parameterization of the generalized gradient approximation (GGA). In order to overcome the well-known band gap issues of TiO_2, we employed the GGA+U method to treat the 3d electrons of Ti [42], which provides an intrinsic band gap of 3.1 eV of the bulk anatase TiO_2 for U = 7.0. In order to avoid interactions between the slabs, a vacuum of more than 15 Å is introduced in the model. A Γ-centered 3 × 3 × 1 Monkhorst–Pack [43] k-point mesh was employed for the Brillion zone sampling of the 4 × 4 supercell. The outermost s- and p-electrons of Bi and O, and s-, p-, and d-electrons of Ti were considered for the valence states in the PAW potentials. The energy cut-off of the plane wave basis was set to 400 eV. The electronic minimization was performed using a tolerance of 10^{-4} eV, while the ionic relaxation was performed using a force tolerance of 0.01 eV/Å for each ion. All these parameters were carefully tested to ensure convergence and accuracy.

Acknowledgements

This work was financially supported by the National Basic Research Program of China (No. 2015CB932302), National Natural Science Foundation of China (Nos. U1432133, 11621063, 21701164, and 11374273), National Program for Support of Top-notch Young Professionals and the Fundamental Research Funds for the Central Universities (Nos. WK2060190084, WK2060190058, and WK2340000063). We also appreciate the support from the Major/Innovative Program of Development Foundation of Hefei Center for Physical Science and Technology.

Electronic Supplementary Material: Supplementary material (TEM images, XRD, PL and EXAFS results) is available in the online version of this article at https://doi.org/10.1007/s12274-017-1933-4.

References

[1] Lin, S.; Diercks, C. S.; Zhang, Y. B.; Kornienko, N.; Nichols, E. M.; Zhao, Y. B.; Paris, A. R.; Kim, D.; Yang, P. D.; Yaghi,

O. M. et al. Covalent organic frameworks comprising cobalt porphyrins for catalytic CO_2 reduction in water. *Science* **2015**, *349*, 1208–1213.

[2] Schneider, J.; Jia, H. F.; Muckerman, J. T.; Fujita, E. Thermodynamics and kinetics of CO_2, CO, and H^+ binding to the metal centre of CO_2 reduction catalysts. *Chem. Soc. Rev.* **2012**, *41*, 2036–2051.

[3] Wang, W. H.; Himeda, Y.; Muckerman, J. T.; Manbeck, G. F.; Fujita, E. CO_2 hydrogenation to formate and methanol as an alternative to photo- and electrochemical CO_2 reduction. *Chem. Rev.* **2015**, *115*, 12936–12973.

[4] Ouyang, T.; Huang, H. H.; Wang, J. W.; Zhong, D. C.; Lu, T. B. A dinuclear cobalt cryptate as a homogeneous photocatalyst for highly selective and efficient visible–light driven CO_2 reduction to CO in CH_3CN/H_2O solution. *Angew. Chem., Int. Ed.* **2017**, *56*, 738–743.

[5] Neaţu, Ş.; Maciá-Agulló, J. A.; Concepción, P.; Garcia, H. Gold–copper nanoalloys supported on TiO_2 as photocatalysts for CO_2 reduction by water. *J. Am. Chem. Soc.* **2014**, *136*, 15969–15976.

[6] Zhao, C. M.; Dai, X. Y.; Yao, T.; Chen, W. X.; Wang, X. Q.; Wang, J.; Yang, J.; Wei, S. Q.; Wu, Y.; Li, Y. D. Ionic exchange of metal-organic frameworks to access single nickel sites for efficient electroreduction of CO_2. *J. Am. Chem. Soc.* **2017**, *139*, 8078–8081.

[7] Chang, X. X.; Wang, T.; Zhang, P.; Wei, Y. J.; Zhao, J. B.; Gong, J. L. Stable aqueous photoelectrochemical CO_2 reduction by a Cu_2O dark cathode with improved selectivity for carbonaceous products. *Angew. Chem., Int. Ed.* **2016**, *55*, 8840–8845.

[8] Wang, W. N.; An, W. J.; Ramalingam, B.; Mukherjee, S.; Niedzwiedzki, D. M.; Gangopadhyay, S.; Biswas, P. Size and structure matter: Enhanced CO_2 photoreduction efficiency by size-resolved ultrafine Pt nanoparticles on TiO_2 single crystals. *J. Am. Chem. Soc.* **2012**, *134*, 11276–11281.

[9] Ong, W. J.; Tan, L. L.; Chai, S. P.; Yong, S. T.; Mohamed, A. R. Self-assembly of nitrogen-doped TiO_2 with exposed {001} facets on a graphene scaffold as photo-active hybrid nanostructures for reduction of carbon dioxide to methane. *Nano Res.* **2014**, *7*, 1528–1547.

[10] Liu, X.; Inagaki, S.; Gong, J. L. Heterogeneous molecular systems for photocatalytic CO_2 reduction with water oxidation. *Angew. Chem., Int. Ed.* **2016**, *55*, 14924–14950.

[11] Akimov, A. V.; Asahi, R.; Jinnouchi, R.; Prezhdo, O. V. What makes the photocatalytic CO_2 reduction on N-doped Ta_2O_5 efficient: Insights from nonadiabatic molecular dynamics. *J. Am. Chem. Soc.* **2015**, *137*, 11517–11525.

[12] Li, H. Y.; Gan, S. Y.; Wang, H. Y.; Han, D. X.; Niu, L. Intercorrelated superhybrid of AgBr supported on graphitic-C_3N_4-decorated nitrogen-doped graphene: High engineering photocatalytic activities for water purification and CO_2 reduction. *Adv. Mater.* **2015**, *27*, 6906–6913.

[13] Huang, J. H.; Shang, Q. C.; Huang, Y. Y.; Tang, F. M.; Zhang, Q.; Liu, Q. H.; Jiang, S.; Hu, F. C.; Liu, W.; Luo, Y. et al. Oxyhydroxide nanosheets with highly efficient electron–hole pair separation for hydrogen evolution. *Angew. Chem., Int. Ed.* **2016**, *55*, 2137–2141.

[14] Tan, C. L.; Zhang, H. Two-dimensional transition metal dichalcogenide nanosheet-based composites. *Chem. Soc. Rev.* **2015**, *44*, 2713–2731.

[15] Li, J.; Zhan, G. M.; Yu, Y.; Zhang, L. Z. Superior visible light hydrogen evolution of Janus bilayer junctions via atomic-level charge flow steering. *Nat. Commun.* **2016**, *7*, 11480.

[16] Lu, Q. P.; Yu, Y. F.; Ma, Q. L.; Chen, B.; Zhang, H. 2D Transition-metal-dichalcogenide-nanosheet-based composites for photocatalytic and electrocatalytic hydrogen evolution reactions. *Adv. Mater.* **2016**, *28*, 1917–1933.

[17] Bi, W. T.; Li, X. G.; Zhang, L.; Jin, T.; Zhang, L. D.; Zhang, Q.; Luo, Y.; Wu, C. Z.; Xie, Y. Molecular co-catalyst accelerating hole transfer for enhanced photocatalytic H_2 evolution. *Nat. Commun.* **2015**, *6*, 8647.

[18] Liu, G. G.; Wang, T.; Zhang, H. B.; Meng, X. G.; Hao, D.; Chang, K.; Li, P.; Kako, T.; Ye, J. H. Nature-inspired environmental "phosphorylation" boosts photocatalytic H_2 production over carbon nitride nanosheets under visible-light irradiation. *Angew. Chem., Int. Edit.* **2015**, *54*, 13561–13565.

[19] Deng, D. H.; Novoselov, K. S.; Fu, Q.; Zheng, N. F.; Tian, Z. Q.; Bao, X. H. Catalysis with two-dimensional materials and their heterostructures. *Nat. Nanotechnol.* **2016**, *11*, 218–230.

[20] Guo, Y. Q.; Xu, K.; Wu, C. Z.; Zhao, J. Y.; Xie, Y. Surface chemical-modification for engineering the intrinsic physical properties of inorganic two-dimensional nanomaterials. *Chem. Soc. Rev.* **2015**, *44*, 637–646.

[21] Chou, S. S.; De, M.; Kim, J.; Byun, S.; Dykstra, C.; Yu, J.; Huang, J. X.; Dravid, V. P. Ligand conjugation of chemically exfoliated MoS_2. *J. Am. Chem. Soc.* **2013**, *135*, 4584–4587.

[22] Zhu, X. J.; Guo, Y. Q.; Cheng, H.; Dai, J.; An, X. D.; Zhao, J. Y.; Tian, K. Z.; Wei, S. Q.; Zeng, X. C.; Wu, C. Z. et al. Signature of coexistence of superconductivity and ferromagnetism in two-dimensional $NbSe_2$ triggered by surface molecular adsorption. *Nat. Commun.* **2016**, *7*, 11210.

[23] Mi, S. Y.; Liu, Y. X.; Wang, W. D. Photo-depositing Ru and RuO_2 on anatase TiO_2 nanosheets as Co-catalysts for photocatalytic O_2 evolution from water oxidation. *Chin. J. Chem. Phys.* **2016**, *29*, 585–590.

[24] Fan, Z. X.; Huang, X.; Han, Y.; Bosman, M.; Wang, Q. X.; Zhu, Y. H.; Liu, Q.; Li, B.; Zeng, Z. Y.; Wu, J. et al. Surface modification-induced phase transformation of hexagonal close-packed gold square sheets. *Nat. Commun.* **2015**, *6*, 6571.

[25] Liu, P. X.; Zhao, Y.; Qin, R. X.; Mo, S. G.; Chen, G. X.; Gu, L.; Chevrier, D. M.; Zhang, P.; Guo, Q.; Zang, D. D. et al. Photochemical route for synthesizing atomically dispersed palladium catalysts. *Science* **2016**, *352*, 797–800.

[26] Li, X. G.; Bi, W. T.; Zhang, L.; Tao, S.; Chu, W. S.; Zhang, Q.; Luo, Y.; Wu, C. Z.; Xie, Y. Single-atom Pt as Co-catalyst for enhanced photocatalytic H_2 evolution. *Adv. Mater.* **2016**, *28*, 2427–2431.

[27] Ji, S. F.; Chen, Y. J.; Fu, Q.; Chen, Y. F.; Dong, J. C.; Chen, W. X.; Li, Z.; Wang, Y.; Gu, L.; He, W. et al. Confined pyrolysis within metal–organic frameworks to form uniform Ru_3 clusters for efficient oxidation of alcohols. *J. Am. Chem. Soc.* **2017**, *139*, 9795–9798.

[28] Qiao, B. T.; Wang, A. Q.; Yang, X. F.; Allard, L. F.; Jiang, Z.; Cui, Y. T.; Liu, J. Y.; Li, J.; Zhang, T. Single-atom catalysis of CO oxidation using Pt_1/FeO_x. *Nat. Chem.* **2011**, *3*, 634–641.

[29] Kronik, L.; Shapira, Y. Surface photovoltage phenomena: Theory, experiment, and applications. *Surf. Sci. Rep.* **1999**, *37*, 1–206.

[30] Lu, Y. C.; Lin, Y. H.; Wang, D. J.; Wang, L. L.; Xie, T. F.; Jiang, T. F. A high performance cobalt-doped ZnO visible light photocatalyst and its photogenerated charge transfer properties. *Nano Res.* **2011**, *4*, 1144–1152.

[31] Liu, Z. Y.; Sun, D. D.; Guo, P.; Leckie, J. O. An efficient bicomponent TiO_2/SnO_2 nanofiber photocatalyst fabricated by electrospinning with a side-by-side dual spinneret method. *Nano Lett.* **2007**, *7*, 1081–1085.

[32] Li, H. Y.; Wang, D. J.; Fan, H. M.; Jiang, T. F.; Li, X. L.; Xie, T. F. Synthesis of ordered multivalent Mn-TiO_2 nanospheres with tunable size: A high performance visible-light photocatalyst. *Nano Res.* **2011**, *4*, 460–469.

[33] Xin, B. F.; Jing, L. Q.; Ren, Z. Y.; Wang, B. Q.; Fu, H. G. Effects of simultaneously doped and deposited Ag on the photocatalytic activity and surface states of TiO_2. *J. Phys. Chem. B* **2005**, *109*, 2805–2809.

[34] Peng, L. L.; Xie, T. F.; Lu, Y. C.; Fan, H. M.; Wang, D. J. Synthesis, photoelectric properties and photocatalytic activity of the Fe_2O_3/TiO_2 heterogeneous photocatalysts. *Phys. Chem. Chem. Phys.* **2010**, *12*, 8033–8041.

[35] Gross, D.; Mora-Sero, I.; Dittrich, T.; Belaidi, A.; Mauser, C.; Houtepen, A. J.; Da Como, E.; Rogach, A. L.; Feldmann, J. Charge separation in type II tunneling multilayered structures of CdTe and CdSe nanocrystals directly proven by surface photovoltage spectroscopy. *J. Am. Chem. Soc.* **2010**, *132*, 5981–5983.

[36] Habisreutinger, S. N.; Schmidt-Mende, L.; Stolarczyk, J. K. Photocatalytic reduction of CO_2 on TiO_2 and other semiconductors. *Angew. Chem., Int. Ed.* **2013**, *52*, 7372–7408.

[37] Han, X. G.; Kuang, Q.; Jin, M. S.; Xie, Z. X.; Zheng, L. S. Synthesis of titania nanosheets with a high percentage of exposed (001) facets and related photocatalytic properties. *J. Am. Chem. Soc.* **2009**, *131*, 3152–3153.

[38] Kresse, G.; Furthmüller, J. Efficient iterative schemes for *ab initio* total-energy calculations using a plane-wave basis set. *Phys. Rev. B* **1996**, *54*, 11169–11186.

[39] Blöchl, P. E. Projector augmented-wave method. *Phys. Rev. B* **1994**, *50*, 17953–17979.

[40] Kresse, G.; Joubert, D. From ultrasoft pseudopotentials to the projector augmented-wave method. *Phys. Rev. B* **1999**, *59*, 1758–1775.

[41] Perdew, J. P.; Burke, K.; Ernzerhof, M. Generalized gradient approximation made simple. *Phys. Rev. Lett.* **1996**, *77*, 3865–3868.

[42] Anisimov, V. I.; Zaanen, J.; Andersen, O. K. Band theory and Mott insulators: Hubbard *U* instead of stoner *I*. *Phys. Rev. B* **1991**, *44*, 943–954.

[43] Methfessel, M.; Paxton, A. T. High-precision sampling for Brillouin-zone integration in metals. *Phys. Rev. B* **1989**, *40*, 3616–3621.